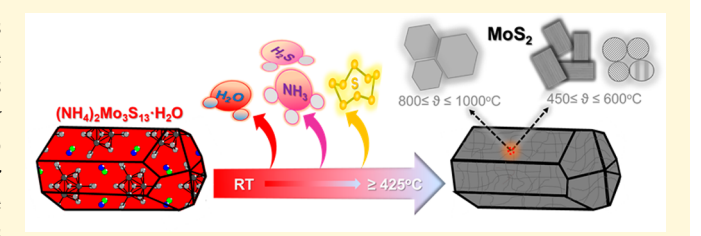
# Conversion of Single Crystal (NH<sub>4</sub>)<sub>2</sub>Mo<sub>3</sub>S<sub>13</sub>·H<sub>2</sub>O to Isomorphic Pseudocrystals of MoS<sub>2</sub> Nanoparticles

Saiful M. Islam, †, Lintao Peng, | Abhishek Banerjee, † 
Kota S. Subrahmanyam, † Yuan Li, † Shulan Ma, \* Vinayak P. Dravid, †, 8 Matthew Grayson, | and Mercouri G. Kanatzidis\*,†

# Supporting Information

ABSTRACT: We have prepared nanocrystals of MoS<sub>2</sub> across a range of length scales by heating single crystals of the molecular precursor (NH<sub>4</sub>)<sub>2</sub>Mo<sub>3</sub>S<sub>13</sub>·H<sub>2</sub>O. Rod-shaped crystals of the polysulfide precursor retain their original morphology after heating at temperatures up to 1000 °C and undergo complete conversion to MoS2 while acting as a template for the confined formation of MoS<sub>2</sub> nanocrystals. This solid state transformation proceeds with the release of gaseous species without blowing the crystals apart and leads to formation of



pores embedded into a nanocrystalline assembly of the templated nano-MoS2. The obtained assemblies of MoS2 nanocrystals have the exact same shape of the original rod-shaped (NH<sub>4</sub>)<sub>2</sub>Mo<sub>3</sub>S<sub>13</sub>·H<sub>2</sub>O crystals indicative of a pseudomorphic shape-retentive process. Such crystal-shaped nanocrystal assemblies show electrical conductivity values similar to a bulk MoS<sub>2</sub> single crystal with electron carrier concentration of 1.5  $\times$  10<sup>14</sup> cm<sup>-3</sup> and mobility of 7 cm<sup>2</sup>/(V s). The nanocrystals of MoS<sub>2</sub> were grown at temperatures ranging from 450 to 1000 °C, and the sizes, shapes, morphologies, and their orientations can be engineered as a function of heating rate, soaking time, and temperature. These findings suggest a unique process for constrained templated nanocrystal growth from an organized molecular precursor structure with control of bulk morphology, size distribution, and orientation of nanocrystallites.

# ■ INTRODUCTION

Molybdenum disulfide (MoS<sub>2</sub>) is of great interest for a wide variety of technological applications ranging from electronics to heterogeneous catalysis. 1-4 When the size of this material is reduced to the nanoscale, low-dimensional surface defects such as edges, corners, and kinks become dominant and define the electronic structure of the nanoparticles, which results in tunable optoelectronic properties and highly dense active catalytic sites. 1,5,6 For this reason, focus is centered on the synthesis of MoS2 nanocrystals, with defined sizes, morphologies, stoichiometry, atomic ordering, and microstructures. A great variety of synthetic methods have been implemented including hydrothermal synthesis,<sup>7,8</sup> electrochemical deposition,<sup>9</sup> pulsed laser ablation,<sup>10–12</sup> microwave,<sup>13,14</sup> molten salt synthesis,<sup>15,16</sup> physical vapor deposition,<sup>1,17</sup> chemical vapor deposition (CVD), <sup>18-22</sup> thermal decomposition, <sup>23,24,32,33</sup> metal-organic chemical vapor deposition (MOCVD),<sup>25</sup> solgel methods, 26,27 sonochemical synthesis, 20,21 and chemical and mechanical exfoliation. 28,29 These methods yield MoS<sub>2</sub> nanocrystals with a variety of sizes and shapes such as hexagonal flakes, inorganic fullerene (IF)-like particles, nanotubes, nanorods, nanoflowers, nanowires, microspheres, hollow

spheres, and porous irregularly shaped nanoparticle. 26,30-36 Despite such great advancements in the nanoscopic synthesis of MoS<sub>2</sub>, up to now, solid state assembly of MoS<sub>2</sub> nanocrystals emerging from a single crystal molecular precursor as template to obtain porous isomorphic pseudocrystals of assembled MoS<sub>2</sub> nanoparticles is not known in the literature.

Herein, we report a direct high temperature (450 °C  $\leq T \leq$ 1000 °C) solid state reaction that leads to MoS<sub>2</sub> nanocrystals with controllable sizes, shapes, morphologies, and orientations. This is a unique solvent-free, scalable process that uses crystals of the molecular precursor  $(NH_4)_2[Mo_3S(S_2)_6]\cdot H_2O$  which features a trinuclear cluster<sup>37</sup> (see Figure 1A). Generally, high temperature conversion processes lead to large crystals and are not regarded as suitable routes toward nanomaterials synthesis. We show that the crystal structure of the chemically homogeneous solid precursor of hydrous (NH<sub>4</sub>)<sub>2</sub>[Mo<sub>3</sub>S- $(S_2)_6$  ]· $H_2O$  is unique in that upon heating it enables the rapid but orderly topotactic removal of H<sub>2</sub>O molecules to give

Received: March 25, 2018 Revised: May 21, 2018 Published: May 21, 2018

3847

<sup>&</sup>lt;sup>†</sup>Department of Chemistry, <sup>‡</sup>Materials Science and Engineering, <sup>§</sup>International Institute for Nanotechnology, and <sup>||</sup>Applied Physics Graduate Program, Northwestern University, Evanston, Illinois 60208, United States

<sup>&</sup>lt;sup>1</sup>Department of Chemistry, Physics, and Atmospheric Sciences, Jackson State University, Jackson, Mississippi 39217, United States \*College of Chemistry, Beijing Normal University, Beijing 100875, China

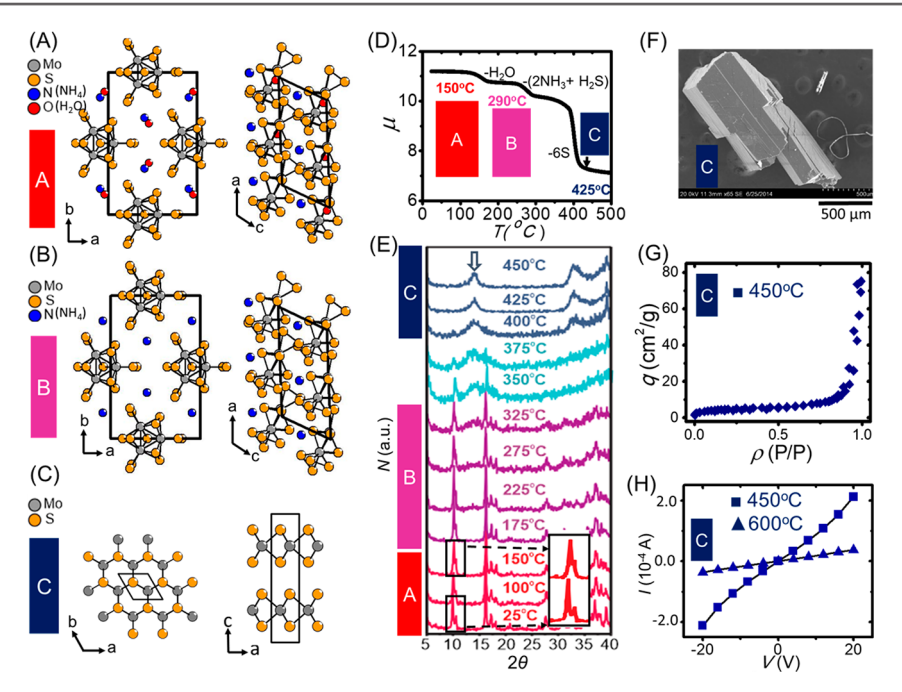


Figure 1. (A, B, C) Side by side comparison of the crystal structures of hydrous  $(NH_4)_2Mo_3S_{13}$ ·H<sub>2</sub>O, anhydrous  $(NH_4)_2Mo_3S_{13}$ , and  $MoS_2$  represented by A (red), B (pink), and C (blue) bars, respectively, for the successive figures. In (B), the absence of oxygen atoms depicted by the red circles corresponds to the absence of water molecules after heating to ~300 °C. (D) Thermogravimetric analysis of hydrous  $(NH_4)_2Mo_3S_{13}$ ·H<sub>2</sub>O shows fraction of mass loss,  $\mu$ , by the release of H<sub>2</sub>O,  $2NH_3 + H_2S$ , and S at temperatures, T, of 150, 290, and 425 °C, respectively. (E) In situ powder diffraction tracts the route of the conversion of  $(NH_4)_2Mo_3S_{13}$ ·H<sub>2</sub>O to  $MoS_2$ ; (A, B, and C) bars represent the compounds corresponding to Figures A, B, and C. Inset in Figure E shows the shifting of the powder diffraction pattern with temperature; downward arrows indicate the formation of  $MoS_2$ . (F) Nanocrystalline assembly of  $MoS_2$  single crystalline pseudomorph formed by heating in a templated fashion starting a single crystal of  $(NH_4)_2Mo_3S_{13}$ ·H<sub>2</sub>O; see eq 1. (G) BET surface area of the molybdenum disulfides pseudomorph prepared at 450 °C as represented in Figure F. (H) Comparison of the I-V curve of self-assembled nanocrystals into the isomorphic pseudocrystal of  $MoS_2$  prepared at 450 and 600 °C.

anhydrous  $(NH_4)_2[Mo_3S(S_2)_6]$  (Figure 1B) and the subsequent removal of  $NH_3$ ,  $H_2S$ , and sulfur gas without destruction of the original crystal shape. The starting molecular crystals transform into crystals of identical shapes (pseudomorphs) but composed of porous assemblies of nanocrystalline layered  $MoS_2$  (Figure 1C). In the present case we showed a spatially constrained solvent free process leading to a unique process for the synthesis of well-defined porous pseudomorphs. In addition, we showed that such high temperature solid state synthesis lead nanocrystals with fewer defect that can exhibit interesting optoelectronic properties.

# RESULTS AND DISCUSSION

Red single crystals of the hydrous  $(NH_4)_2[Mo_3S(S_2)_6]\cdot H_2O$  precursor, up to centimeter scales, were synthesized by heating an aqueous mixture of  $(NH_4)_6Mo_7O_{24}\cdot 4H_2O$ ,  $NH_2OH\cdot HCl$ , and  $(NH_4)_2S_x$  in an autoclave using a modified Mueller's method<sup>37</sup> (see Supporting Information for the detailed modified synthesis). Our study revealed that the compound can be synthesized at temperatures ranging from 90 to 220 °C. A yield of nearly ~100% (based on Mo content in  $(NH_4)_6Mo_7O_{24}\cdot 4H_2O)$  was obtained via a reaction at 220 °C over a period of 48 h, and thus this procedure is superior to Mueller's, <sup>37</sup> which yields ~20%.

The thermal behavior of hydrous  $(NH_4)_2[Mo_3S(S_2)_6]\cdot H_2O$  with increasing temperature was studied by thermogravimetric analysis (TGA) (Figure 1D, fraction of mass,  $\mu$  with temperature, T) and in situ X-ray powder diffraction (Figure 1E). The TGA curve reveals that this molecule transforms from the hydrous to anhydrous state at approximately 160 °C, which then remains steady until ~300 °C, signifying an impressive

thermal stability of the anhydrous molecule,  $(NH_4)_2[Mo_3S-(S_2)_6].$  Subsequent heating above 300 °C decomposes the anhydrous  $(NH_4)_2[Mo_3S(S_2)_6]$  to  $MoS_2$  at  ${\sim}425$  °C through a gradual loss of volatile gaseous species like  $NH_3,\ H_2S,$  and sulfur or sulfur-containing species. This feature is in agreement with the observation of Mueller et al.  $^{23}$ 

In situ powder X-ray diffraction shows that at approximately 150 °C the diffraction pattern does not change, but the Bragg peaks shift to larger  $2\theta$  (inset in Figure E), demonstrating a contraction of the unit cell volume as a result of the hydrous to anhydrous (NH<sub>4</sub>)<sub>2</sub>[Mo<sub>3</sub>S(S<sub>2</sub>)<sub>6</sub>] transformation. From the *in situ* powder diffraction it can be seen that this polysulfide molecule, remarkably, is stable until 325 °C. This observation is consistent with the TGA, and the slight difference in the decomposition temperature is attributed to the different heating rate (see Supporting Information for a detailed experiment). In fact, this transformation is so orderly that when a single crystal of the hydrous (NH<sub>4</sub>)<sub>2</sub>[Mo<sub>3</sub>S(S<sub>2</sub>)<sub>6</sub>]·H<sub>2</sub>O material is used, a single crystal of the anhydrous version can be obtained which can be used to solve and refine the structure from single crystal X-ray diffraction data as will be presented below.

Subsequent heating at higher temperatures further decomposes the polysulfide molecule, and the crystalline  $(NH_4)_2[Mo_3S(S_2)_6]$  converts to nanocrystalline  $MoS_2$  at about 425 °C through a isomorphic transition occurring between ~350 and ~400 °C. By isomorphic we mean that the original crystals of the precursor retain their full shape even though the molecular compound no longer exists. The disappearance of the original X-ray diffraction pattern and appearance of broad diffraction peaks at  $2\theta$  ~14° along with

others at 425  $^{\circ}\text{C}$  indicate the formation of nanocrystalline MoS<sub>2</sub>.

The chemical environments and oxidation states of Mo, S atoms in the pristine hydrous (NH<sub>4</sub>)<sub>2</sub>Mo<sub>3</sub>S<sub>13</sub>·H<sub>2</sub>O, anhydrous  $(NH_4)_2Mo_3S_{13}\cdot H_2O$  (300 °C heated sample), and the nanocrystalline MoS<sub>2</sub> (450 °C sample) were characterized with Xray photoelectron spectroscopy (Figure S1). As synthesized, (NH<sub>4</sub>)<sub>2</sub>Mo<sub>3</sub>S<sub>13</sub>·H<sub>2</sub>O exhibits the BEs of 228.86 and 232.06 eV for Mo4+ 3d and 164.39-161.86 eV for S 2p. The variability in the BEs of S 2p is attributed to two different oxidation states of as well as the splitting caused by the spin-orbit interaction in the sulfur atoms.<sup>38</sup> Within this range of BEs, the bands at 163.29 and 164.39 eV correspond to the  $S^{1-}$  2p<sub>3/2</sub> and 2p<sub>1/2</sub>, respectively while the bands centered at 161.86 and 162.96 eV correspond to the  $S^{2-}$   $2p_{3/2}$  and  $2p_{1/2}$ , respectively.<sup>39</sup> The change in the BEs of anhydrous (NH<sub>4</sub>)<sub>2</sub>Mo<sub>3</sub>S<sub>13</sub> relative to pristine hydrous is insignificant, as expected. For the MoS<sub>2</sub> formed at 450 °C, the BEs at 230.16 and 233.30 eV correspond to Mo  $3d_{5/2}$  and  $3d_{3/2}$ , respectively, while those at 163.26 and 164.36 eV represent the S  $2p_{3/2}$  and  $2p_{1/2}$ , respectively, and are consistent with literature values. The Raman spectrum of the porous MoS<sub>2</sub> bulk pseudocrystal shows bands centered at ~404 and  $\sim 379$  cm<sup>-1</sup>, which represent the  $A_{1g}$  and  $E_{1g}$ vibrational modes of MoS<sub>2</sub>, respectively (Figure S2).

To validate hydrous to anhydrous single crystal transformation and its structural and compositional resilience, we determined the X-ray single crystal structure of the assynthesized  $(NH_4)_2[Mo_3S(S_2)_6] \cdot H_2O$  and annealed anhydrous crystal at 300 °C (Figure 1A,B). In agreement with Mueller et al., The hydrous  $(NH_4)_2[Mo_3S(S_2)_6] \cdot H_2O$  consists of a  $Mo_3$ triangle in which two molybdenum atoms are bridged by disulfide groups,  $(S_2^{2-})_{\text{bridge}}$  so-called bridging sulfur, and an epical  $(S^{2-})_{\text{epical}}$  (monosulfide group) in addition to a terminal  $(S_2^{2-})_{term}$  group on each Mo. This molecular complex is stabilized by the (NH<sub>4</sub>)<sup>+</sup> counterions besides the neutral crystal water. The crystal structure of the 300 °C annealed crystal is similar but shows a decreased unit cell size and the absence of H<sub>2</sub>O molecules, which is in agreement with the TGA and in situ X-ray powder diffraction experiments. The unit cell parameters of the anhydrous NH<sub>4</sub>)<sub>2</sub>[Mo<sub>3</sub>S(S<sub>2</sub>)<sub>6</sub>] are a = 11.5136(23), b =16.3569(33), c = 5.7209(11) Å,  $\beta = 117.746(30)^{\circ}$ , and V =953.52(42) Å<sup>3</sup>, which are smaller than the hydrous version, with unit cell parameters a = 11.5673(23) Å, b = 16.4189(33)Å, c = 5.7049(11) Å,  $\beta = 117.366(30)^{\circ}$ , and V = 962.23(42) Å<sup>3</sup>.

When the single crystals of anhydrous  $(NH_4)_2[Mo_3S(S_2)_6]$  are heated further, they convert to a rigid assembly of 2D  $MoS_2$  nanocrystals, preserving the morphology of the original single crystals (Figure 1F and Figure S3). Despite severe compositional and structural differences between the 0D molecular polysulfide and the layered  $MoS_2$  and the large amount of escaping gaseous species  $(H_2O, NH_3, H_2S,$  and sulfur), according to eq 1, it is truly remarkable that the conversion of hydrous  $(NH_4)_2[Mo_3S(S_2)_6]\cdot H_2O$  to  $MoS_2$  retains the bulk morphology inherited from the host crystal (Figure 1F).

$$(NH_4)_2 Mo_3 S_{13} H_2 O \xrightarrow{-H_2 O}_{\sim 170 \text{ °C}} (NH_4)_2 Mo_3 S_{13}$$

$$\xrightarrow{-2NH_3 + H_2 S}_{\sim 300 \text{ °C}} [Mo_3 S_{12}] \rightarrow 3MoS_2$$
(1)

Thus, the single crystals of  $(NH_4)_2[Mo_3S(S_2)_6]\cdot H_2O$  afford a robust template for the growth nanocrystalline  $MoS_2$  without the crystal "exploding" from the violent expulsion of gases during the conversion (Figure S2). We could hypothesize the

phenomena as the decomposition proceeds from hydrous to anhydrous (NH<sub>4</sub>)<sub>2</sub>Mo<sub>3</sub>S<sub>13</sub> which subsequently can undergo further degradation by the liberation of NH<sub>3</sub> while the H<sup>+</sup> ion can act as counterions to charge balance and may from a onedimensional chain. Further heating loses H<sub>2</sub>S and S along with a simultaneous and very fast diffusion of the atoms Mo and S to form thermodynamically stable a two-dimensional structure of MoS<sub>2</sub>. Therefore, the underlying reason may be the details of the parent crystal structure of  $(NH_4)_2Mo_3S_{13}\cdot H_2O$  which may allow facile escape of gas molecule and thus reveal the isomorphic structure of the host crystal. SEM images show the presence of nanoscale cracks and pores which originate from the escape of gaseous species as indicated by eq 1. Despite these cracks and pores, the pseudocrystals of the MoS<sub>2</sub> ensembles are found to be nearly mechanically as stable and sustain upon general handling in the lab. Such mechanical stability could be the result of the formation of interlocking assembly of the aggregated nanocrystallites that themselves interact and define a 3D porous matrix. The porosity in the pseudocrystals was further validated with surface area measurements, giving  $\sim 18 \text{ m}^2/\text{g}$ , where the adsorption average pore width by BET is 264.5 Å and pore volume is 0.12 cm<sup>3</sup>/g for the porous bulk crystals of MoS<sub>2</sub> prepared at 450 °C (heating rate 150 °C/h for ramp up and down and soaked for 2 h) (Figure 1G, quantity of absorbed gas, q, against relative pressure,  $\rho$ ). This value is higher than the 13 m<sup>2</sup>/g, which has been reported for the thermal decomposition of similar precursor at 400 °C. 41 However, ultrasonic pyrolysis of (NH<sub>4</sub>)<sub>2</sub>MoS<sub>4</sub> to MoS<sub>2</sub> without template led to BET surface area of 20-40 m<sup>2</sup>/g, but in the presence of  ${\rm SiO_2}$  template this synthesis procedure led to a maximum surface area of 250 m<sup>2</sup>/g.<sup>42</sup>

The rigidity of the nanocrystal assemblies allowed electrical resistivity measurements to be conducted on the entire porous pseudocrystals obtained at 450 and 600 °C (heating rate 15 °C/m, soaking time 1 h) (see Figure 1H). Relatively low resistivities,  $\rho \sim 6.36 \times 10^3 \ \Omega \cdot \text{cm}$  (conductivity,  $\sigma \sim 1.58 \times 10^3 \ \Omega \cdot \text{cm}$  $10^{-4} \, \mathrm{S \ cm}^{-1}$ ) and  $\rho \sim 5.46 \times 10^4 \, \Omega \cdot \mathrm{cm}$  (conductivity,  $\sigma \sim 1.83$  $\times$  10<sup>-5</sup> S cm<sup>-1</sup>) were measured for the 450 and 600 °C MoS<sub>2</sub>, respectively. These results show the electrical conductivity of 450 °C samples is approximately 1 order magnitude higher than that of the 600 °C samples. This is consistent with a smaller average particle size and better electrical connectivity of the particles. Higher temperature could also lead to directional diffusion of the atoms at certain grain boundaries, resulting in an increase of the density of pores in the bulk pseudocrystal. Interestingly, the electrical conductivities of such porous pseudosingle crystals exhibit very close to the value obtained for single bulk crystals of MoS<sub>2</sub> along the *c*-axis ( $\sigma \sim 4.6 \times 10^{-4}$ S cm<sup>-1</sup>).<sup>43</sup> This finding clearly suggests that despite the high density of pores the aggregated MoS2 nanoparticles form a 3D network throughout the pseudosingle crystal. In addition, such solid-state conversion leads to high crystal quality of the MoS<sub>2</sub> nanocrystals, and their conjoining feature allows facile charge transport across the pseudomorph crystals. The Hall resistance of the porous bulk pseudomorph crystal obtained at 450 °C was measured at 300 K, showing n-type conduction (Figure S4). The nominal carrier density of electrons is  $n = (1.5 \pm 0.2)$  $\times$  10<sup>14</sup> cm<sup>-3</sup> with carrier mobility of 7 ± 1 cm<sup>2</sup>/(V s).

The sizes, shapes, morphologies, and orientations of the MoS<sub>2</sub> nanocrystallites inside the pseudocrystals were studied as a function of processing temperature, ramp rate, and annealing duration. The nanocrystallites of MoS<sub>2</sub> were then studied by transmission electron microscopy (TEM), scanning electron

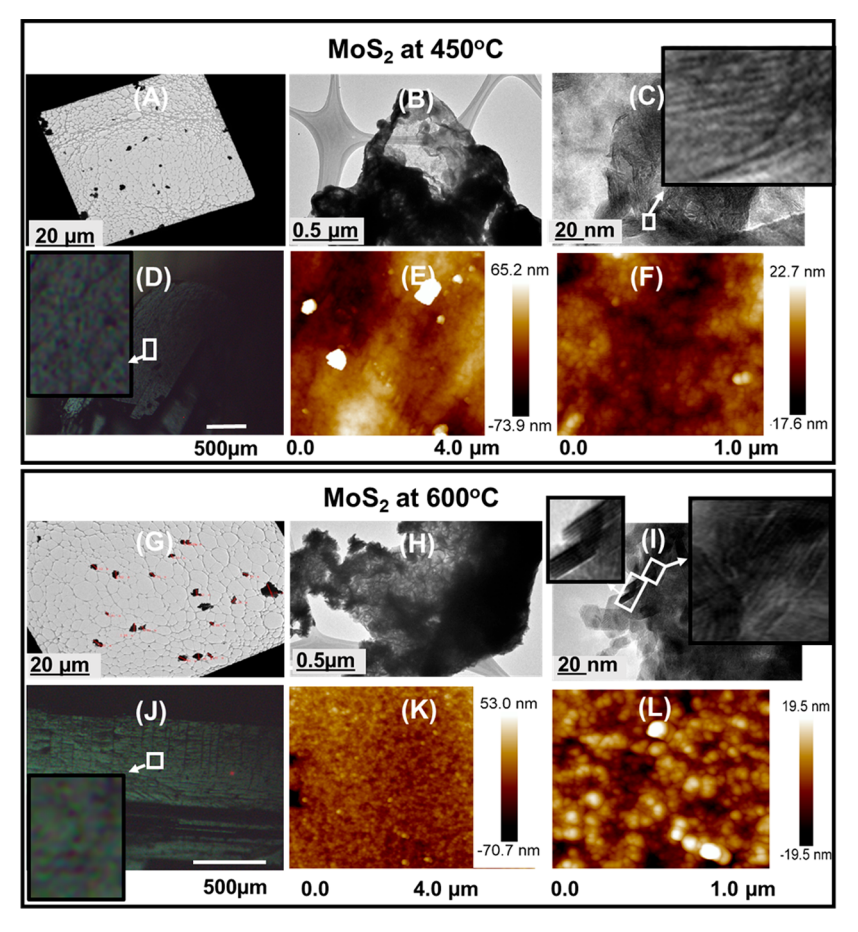


Figure 2. TEM and AFM images of the MoS<sub>2</sub> synthesized at 450 and 600 °C. (A) TEM shows chunky aggregated MoS<sub>2</sub> particles represented by black small objects, obtained from the sample synthesized at 450 °C after ultrasonication. (B) TEM image of MoS<sub>2</sub> does not show discrete grains. (C) TEM reveals "edge-on" view showing features of the aggregated nanocrystals; inset shows disordered stacking and presence of dislocation in the MoS<sub>2</sub>. (D) Optical image of the pseudocrystal of MoS<sub>2</sub> obtained at 450 °C captured by AFM; inset shows rough and porous surface of the pseudocrystal. (E, F) AFM images at different magnification exhibiting the irregular morphology of MoS<sub>2</sub>. (G) TEM image of aggregated MoS<sub>2</sub> nanoparticles represented by black small objects, obtained from the sample synthesized at 600 °C. (H) TEM image of MoS<sub>2</sub> shows evidence of the formation of individual grains. (I) Low-magnification TEM image shows disordered "edge-on" features in the MoS<sub>2</sub> with stacking of the 6–12 layer of basal planes with edge length up to ~40 nm; inset show ordered (left) and disordered (right) features of the crystallites. (J) Optical images of the bulk MoS<sub>2</sub> crystal captured by AFM; inset shows rough and porous surface the pseudocrystal. (K, L) Different magnifications reveal the spherical-like morphology of MoS<sub>2</sub> with estimated particle size ~30 to ~50 nm.

microscopy (SEM), and atomic force microscopy (AFM) (Figures 2 and 3). Single crystals of  $(NH_4)_2[Mo_3S(S_2)_6]\cdot H_2O$  were heated in an evacuated closed silica tube to 450, 600, 800, and 1000 °C with a ramp rate of 15 °C/m and soaked at the respective temperature for 1 h. Subsequently, the empty end of the tube was quenched in water in order to condense the evolved gaseous species and to minimize their adsorption on to the surface of the  $MoS_2$  crystallites. For the TEM analysis, pseudocrystals of  $MoS_2$  were sonicated in EtOH for 2 h to release the particles.

The TEM showed the presence of a highly disorderred aggregrate of nanocryatlline MoS<sub>2</sub> at 450 and 600 °C (Figures 2A–C and 2G–I). High-resolution TEM (HRTEM) images of the nanoaggregates show random 3D orientation and minimal stacking of the plate layers with no visible separation of the flakes. For the samples prepared at 450 °C, basal planes of the MoS<sub>2</sub> exhibit "edge on" features with occasional dislocations (Figure 2C, inset) which often result in surface curvature in the mesostructure of the crystallites. AFM clearly shows (Figure 2D–F) the irregular morphology of the MoS<sub>2</sub> nanoparticles which are aggregated. From AFM images (Figure 2F) the size

of the nanoparticles can be estimated at  $\sim$ 20 to  $\sim$ 30 nm. Figure 2D shows the porous morphology of bulk pseudocrystals. The darker regions of the AFM images (Figure 2E,F) reveal the evidence of porosity created by the loss of volatile gaseous species during the transformation. At 600 °C, TEM images (Figure 2G,H) show no visual separation of MoS<sub>2</sub> flakes but reveal pronouced stacking features of the layers along with disordered features of the lattices (Figure 2I, left inset). HRTEM estimates 6–12 layer stacking along the crystallographis c-axis with the edge length of crystallites being up to  $\sim$ 40 nm. AFM images also show that the nanoparticles exhibit irregular morphologies with nanoparticles of diameter ranging from  $\sim$ 30 to  $\sim$ 50 nm (Figure 2K,L).

Higher processing temperatures (800 and 1000 °C) result in well-ordered stacking of the atoms extending along all the crystallographic directions with growth toward the thermodynamically preferable [002] planes becoming dominant (Figure 3A–D). TEM shows the presence of hexagonal plates which are easily separated upon sonication in EtOH. At 800 °C, the size of the hexagonal flakes range from  $\sim$ 40 to  $\sim$ 150 nm, with the majority of the particles exhibiting edge length between 50

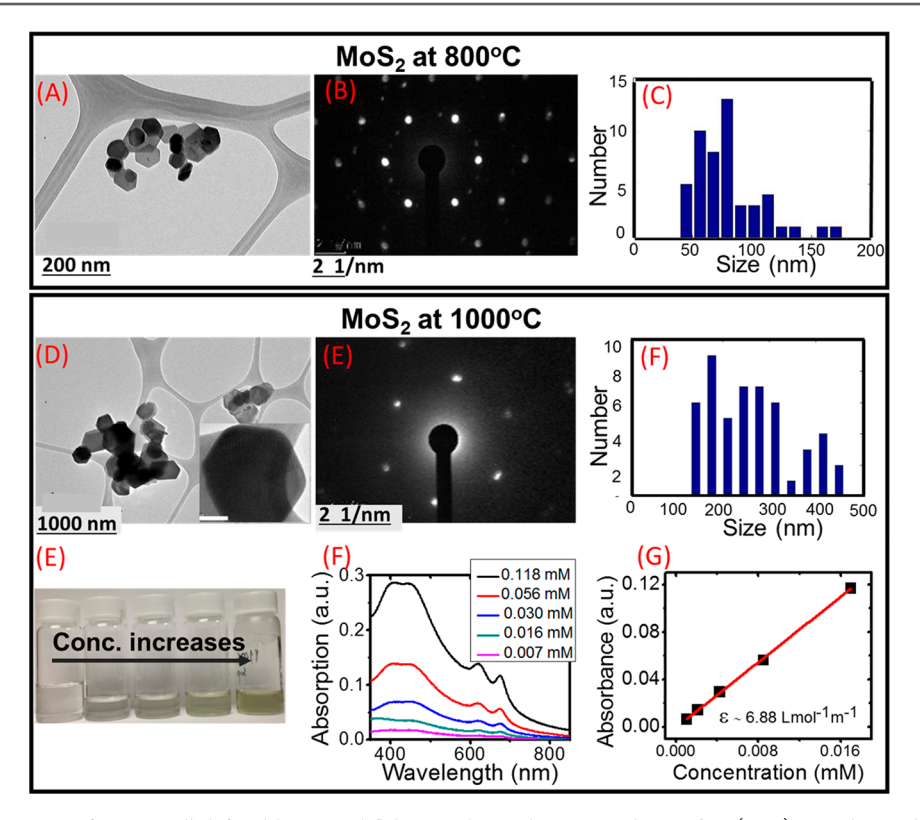
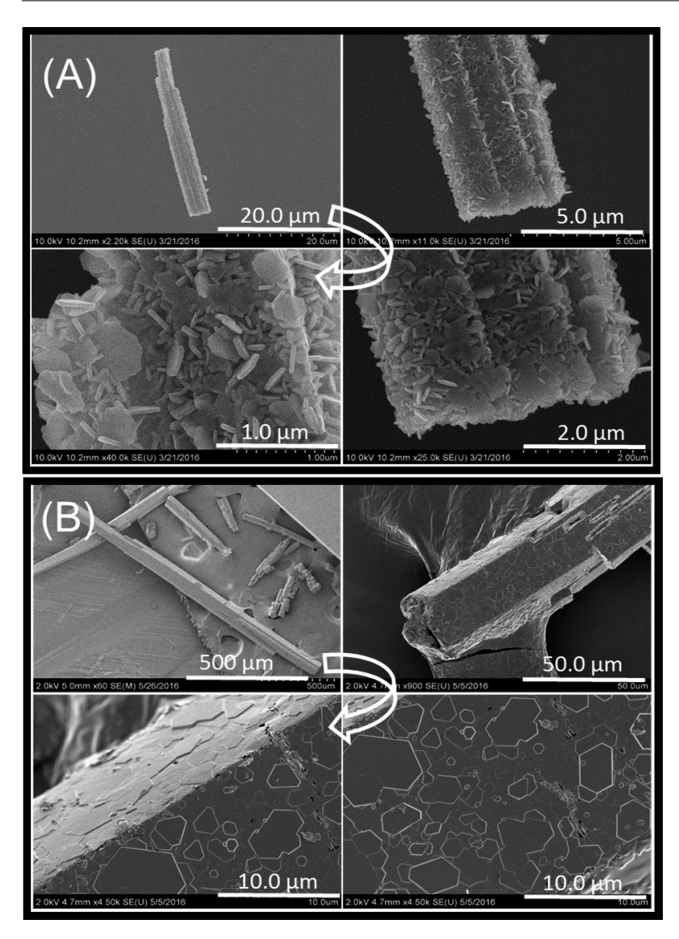


Figure 3. (A, D) TEM images of  $MoS_2$  well-defined hexagonal flakes synthesized at 800 and 1000 °C. (B, E) Nanobeam diffraction pattern of the flakes; (E) obtained from inset flake of (D), white scale bar is 50 nm. (C, F) Statistical size distributions of the  $MoS_2$  determined under TEM from the 800 and 1000 °C samples, respectively. (E) Solution-based exfoliated  $MoS_2$  flakes obtained by centrifugation of the ultrasonicated products at various concentrations. (F) UV/vis absorption spectra of  $MoS_2$  dispersed solutions, showing that intensity of the absorption spectra increases as a function of concentration. (G) Molar absorption coefficient, 6.88 L  $mol^{-1}$   $m^{-1}$ , of  $MoS_2$  solutions determined from absorption vs concentration plots.

and 100 nm (Figure 3C). The sizes of the particles become larger with increased temperature, and at 1000 °C the lateral size of the nanocrystals ranges from ~150 to ~500 nm (Figure 3E). This increase in size is the result of the merging of closely connected smaller crystallites which are fused by solid state diffusion of atoms at elevated temperature (Figure S5). The crystal pseudomorphs have mechanical integrity which supports the notion of sintered conjoining MoS<sub>2</sub> microcrystals. This is supported by the sharper PXRD patterns of the MoS<sub>2</sub> synthesized in the range 450-1000 °C at a heating rate 15 °C/m (Figure S6). It is important to mention that for Figure 1E the PXRD of MoS<sub>2</sub> was collected at high temperature (400-450 °C) during the in situ heating of (NH<sub>4</sub>)<sub>2</sub>Mo<sub>3</sub>S<sub>13</sub>· H<sub>2</sub>O, while the PXRD for the MoS<sub>2</sub> samples in Figure S6 were collected at room temperature. This accounts for the differences in intensity of the diffraction patterns between the two classes of samples; however, the probability of turbostratic stacking and differences in such based on different heating temperatures cannot be ruled out. The well-defined crystals obtained at 1000 °C can exfoliate in isopropanol by ultrasonication (Figure 3H-J). The UV/vis absorption spectra of the supernatant solution of the exfoliated MoS2 nanosheets (Figure 3H) exhibit two pairs of bands: the first pair appears at 675 and 625 nm corresponding to the A and B excitons, while the second intense broad pair centered at 443 and 413 nm corresponds to the C and D excitonic transitions. 28,43,44 The molar extinction coefficient was calculated at ~6.8 L mol<sup>-1</sup> m<sup>-1</sup>. As expected, very similar absorption spectra were observed for the MoS<sub>2</sub> synthesized at 800 °C (Figure S7).

In addition to directing the morphology and size of the nanocrystals, the orientation of the crystallites within the template of the host polysulfide crystal can be controlled. For example, nanocrystals of MoS2 from the host matrix of molybdenum polysulfides (NH<sub>4</sub>)<sub>2</sub>Mo<sub>3</sub>S<sub>13</sub>·H<sub>2</sub>O were formed at 1000 °C with variable heating rates. A rate of 100 °C/h to 1000 °C with a soaking time of 1 h led to intact pseudocrystals composed of well-developed hexagonal plate-like crystallites orientated randomly (Figure 4A). The connectivity at the grain boundaries among the crystallites via fusion is the driving force behind the retention of the original crystal shape. In order to achieve a very slow escape of the gaseous species from the host structure, we heated the precursor crystals at a very slow heating rate, 20 °C/h, to 1000 °C and stayed at this temperature for 6 h. This experiment resulted in pseudocrystals of MoS<sub>2</sub> nanoparticles with different length scales (nanometers to micrometers scale) as well as highly oriented [002] lattice planes of MoS<sub>2</sub> extending along the surface of the host crystal (Figure 4B). This observation could suggest that slower heating rate allows for slower escape of the gaseous species from the host structure, probably creating a common channel to liberate gases, and this eventually could affect the orientation of the crystallites in the host crystal.

This new synthesis strategy for agglomerated assemblies of nanocrystals with specific bulk crystal shapes is a unique route toward nanoscale MoS<sub>2</sub> because it permits much higher processing temperatures and short times while limiting size growth. In addition to this unconventional synthetic technique for porous ensembles of MoS<sub>2</sub>, meticulous control over the



**Figure 4.** Orientation of the crystallites in the pseudocrystal of  $MoS_2$  obtained 1000 °C. (A) Random orientations of the flakes of  $MoS_2$  distributed in structure of host crystal acting as template, obtained at a heating rate of 100 °C/h; the curved arrows indicate different pictures of a same crystal at different magnification. (B)  $MoS_2$  flakes cover the surface of the pseudomorphic crystals, obtained at a very slow heating rate of 20 °C/h.

hierarchical assemblies of the nanocrystals across a range length scales, morphologies, and orientations (within a predetermined template in the form of a starting crystal shape) has not been previously demonstrated.

#### CONCLUSION

In conclusion, crystals of the molecular compound (NH<sub>4</sub>)<sub>2</sub>Mo<sub>3</sub>S<sub>13</sub>·H<sub>2</sub>O are excellent precursors to nanocrystals of MoS<sub>2</sub> as they allow the orderly escape of gases during thermal decomposition to yield an ensemble of agglomerated nanocrystals that retain the shape of the original molecular crystal. Because of the constrained growth conditions in the solid state, the growth of particles is confined in space and can be controlled using the heating rate, soaking time, and temperature. These rigid nanocrystal assemblies show electrical conductivity similar to the bulk single crystal MoS2 which exhibit n-type behavior with electron carrier concentration of  $1.5 \times 10^{14}$  cm<sup>-3</sup> and mobility of 7 cm<sup>2</sup>/(V s). This work elucidates how a chemically homogeneous polysulfide precursor undergoes a transformation from single crystals to isomorphic pseudocrystals of assembled nanoparticles in a porous network. This may enable new opportunities for the synthesis of porous pseudo-single crystals with controllable sizes, shapes, and orientations of the constituent nanocrystals in

constrained growth conditions from similar kinds of molecular precursors. This could be a powerful synthesis strategy for nanomaterials that could be rapidly prepared at higher temperatures and produce more perfect nanomaterials with fewer defects.

## ASSOCIATED CONTENT

## Supporting Information

The Supporting Information is available free of charge on the ACS Publications website at DOI: 10.1021/acs.chemmater.8b01247.

Experimental section and Figures S1–S7 (PDF) Crystallographic files of  $(NH_4)_2Mo_3S_{13}\cdot H_2O$  and  $(NH_4)_2Mo_3S_{13}$  (CIF)

#### AUTHOR INFORMATION

#### **Corresponding Author**

\*E-mail: m-kanatzidis@northwestern.edu (M.G.K.).

#### ORCID ®

Saiful M. Islam: 0000-0001-8518-1856 Yihui He: 0000-0002-1057-6826

Abhishek Banerjee: 0000-0003-4552-4820

Yuan Li: 0000-0001-7452-1149 Shulan Ma: 0000-0002-8326-3134

Vinayak P. Dravid: 0000-0002-6007-3063 Mercouri G. Kanatzidis: 0000-0003-2037-4168

## Notes

The authors declare no competing financial interest.

# ACKNOWLEDGMENTS

S.M.I., M.G.K., V.P.D., and M.G. thank the National Science Foundation for Grant DMR-1720139 (MRSEC program at the Materials Research Center) and Grant 1708254. J.D.C. is supported by the Department of Defense through the National Defense Science and Engineering Fellowship (NDSEG) Program. J.D.C. also gratefully acknowledges support from the Ryan Fellowship and the IIN. SEM, EDS, TEM, Raman, and XPS analyses were performed at the EPIC facility of the NUANCE Center at Northwestern University, supported by NSF-NSEC, NSF-MRSEC, Keck Foundation, the State of Illinois, and Northwestern University. M.G. acknowledges support from AFOSR FA9550-15-1-0247.

# REFERENCES

- (1) Lauritsen, J. V.; Kibsgaard, J.; Helveg, S.; Topsoe, H.; Clausen, B. S.; Laegsgaard, E.; Besenbacher, F. Size-dependent structure of MoS<sub>2</sub> nanocrystals. *Nat. Nanotechnol.* **2007**, *2*, 53–58.
- (2) Gong, Y.; Lin, J.; Wang, X.; Shi, G.; Lei, S.; Lin, Z.; Zou, X.; Ye, G.; Vajtai, R.; Yakobson, B. I.; Terrones, H.; Terrones, M.; Tay, B. K.; Lou, J.; Pantelides, S. T.; Liu, Z.; Zhou, W.; Ajayan, P. M. Vertical and in-plane heterostructures from WS<sub>2</sub>/MoS<sub>2</sub> monolayers. *Nat. Mater.* **2014**, *13*, 1135–1142.
- (3) Li, H.; Tsai, C.; Koh, A. L.; Cai, L.; Contryman, A. W.; Fragapane, A. H.; Zhao, J.; Han, H. S.; Manoharan, H. C.; Abild-Pedersen, F.; Norskov, J. K.; Zheng, X. Activating and optimizing MoS<sub>2</sub> basal planes for hydrogen evolution through the formation of strained sulphur vacancies. *Nat. Mater.* **2016**, *15*, 48–53.
- (4) Sangwan, V. K.; Jariwala, D.; Kim, I. S.; Chen, K. S.; Marks, T. J.; Lauhon, L. J.; Hersam, M. C. Gate-tunable memristive phenomena mediated by grain boundaries in single-layer MoS<sub>2</sub>. *Nat. Nanotechnol.* **2015**, *10*, 403–406.
- (5) Goldstein, A. N.; Echer, C. M.; Alivisatos, A. P. Melting in semiconductor nanocrystals. *Science* **1992**, *256*, 1425–1427.

(6) Wang, Y.; Herron, N. Nanometer-Sized Semiconductor Clusters - Materials Synthesis, Quantum Size Effects, and Photophysical Properties. *J. Phys. Chem.* **1991**, *95*, 525–532.

- (7) Peng, Y. Y.; Meng, Z. Y.; Zhong, C.; Lu, J.; Yu, W. C.; Jia, Y. B.; Qian, Y. T. Hydrothermal synthesis and characterization of single-molecular-layer MoS<sub>2</sub> and MoSe<sub>3</sub>. *Chem. Lett.* **2001**, *30*, 772–773.
- (8) Matte, H. S. S. R.; Gomathi, A.; Manna, A. K.; Late, D. J.; Datta, R.; Pati, S. K.; Rao, C. N. R. MoS<sub>2</sub> and WS<sub>2</sub> Analogues of Graphene. *Angew. Chem., Int. Ed.* **2010**, 49, 4059–4062.
- (9) Li, Q.; Newberg, J. T.; Walter, E. C.; Hemminger, J. C.; Penner, R. M. Polycrystalline molybdenum disulfide (2H-MoS<sub>2</sub>) nano- and microribbons by electrochemical/chemical synthesis. *Nano Lett.* **2004**, 4, 277–281.
- (10) Bar-Sadan, M.; Enyashin, A. N.; Gemming, S.; Popovitz-Biro, R.; Hong, S. Y.; Prior, Y.; Tenne, R.; Seifert, G. Structure and stability of molybdenum sulfide fullerenes. *J. Phys. Chem. B* **2006**, *110*, 25399—25410.
- (11) Enyashin, A. N.; Gemming, S.; Bar-Sadan, M.; Popovitz-Biro, R.; Hong, S. Y.; Prior, Y.; Tenne, R.; Seifert, G. Structure and stability of molybdenum sulfide fullerenes. *Angew. Chem., Int. Ed.* **2007**, *46*, 623–627
- (12) Parilla, P. A.; Dillon, A. C.; Jones, K. M.; Riker, G.; Schulz, D. L.; Ginley, D. S.; Heben, M. J. The first true inorganic fullerenes? *Nature* **1999**, 397, 114–114.
- (13) Ouerfelli, J.; Srivastava, S. K.; Bernede, J. C.; Belgacem, S. Effect of microwaves on synthesis Of MoS<sub>2</sub> and WS<sub>2</sub>. *Vacuum* **2008**, *83*, 308–312.
- (14) Vollath, D.; Szabo, D. V. Synthesis of nanocrystalline MoS<sub>2</sub> and WS<sub>2</sub> in a microwave plasma. *Mater. Lett.* **1998**, 35, 236–244.
- (15) Vanchura, B. A.; He, P. G.; Antochshuk, V.; Jaroniec, M.; Ferryman, A.; Barbash, D.; Fulghum, J. E.; Huang, S. D. Direct synthesis of mesostructured lamellar molybdenum disulfides using a molten neutral n-alkylamine as the solvent and template. *J. Am. Chem. Soc.* 2002, 124, 12090–12091.
- (16) Afanasiev, P.; Rawas, L.; Vrinat, M. Synthesis of dispersed Mo sulfides in the reactive fluxes containing liquid sulfur and alkali metal carbonates. *Mater. Chem. Phys.* **2002**, *73*, 295–300.
- (17) Helveg, S.; Lauritsen, J. V.; Laegsgaard, E.; Stensgaard, I. I.; Norskov, J. K.; Clausen, B. S.; Topsoe, H.; Besenbacher, F. Atomic-scale structure of single-layer  $MoS_2$  nanoclusters. *Phys. Rev. Lett.* **2000**, 84, 951–954.
- (18) Najmaei, S.; Liu, Z.; Zhou, W.; Zou, X.; Shi, G.; Lei, S.; Yakobson, B. I.; Idrobo, J. C.; Ajayan, P. M.; Lou, J. Vapour phase growth and grain boundary structure of molybdenum disulphide atomic layers. *Nat. Mater.* **2013**, *12*, 754–759.
- (19) Lee, Y. H.; Zhang, X. Q.; Zhang, W.; Chang, M. T.; Lin, C. T.; Chang, K. D.; Yu, Y. C.; Wang, J. T.; Chang, C. S.; Li, L. J.; Lin, T. W. Synthesis of large-area MoS<sub>2</sub> atomic layers with chemical vapor deposition. *Adv. Mater.* **2012**, *24*, 2320–2325.
- (20) Liu, K. K.; Zhang, W. J.; Lee, Y. H.; Lin, Y. C.; Chang, M. T.; Su, C.; Chang, C. S.; Li, H.; Shi, Y. M.; Zhang, H.; Lai, C. S.; Li, L. J. Growth of Large-Area and Highly Crystalline MoS<sub>2</sub> Thin Layers on Insulating Substrates. *Nano Lett.* **2012**, *12*, 1538–1544.
- (21) Zhan, Y. J.; Liu, Z.; Najmaei, S.; Ajayan, P. M.; Lou, J. Large-Area Vapor-Phase Growth and Characterization of MoS<sub>2</sub> Atomic Layers on a SiO<sub>2</sub> Substrate. *Small* **2012**, *8*, 966–971.
- (22) Cain, J. D.; Shi, F.; Wu, J.; Dravid, V. P. Growth Mechanism of Transition Metal Dichalcogenide Monolayers: The Role of Self-Seeding Fullerene Nuclei. ACS Nano 2016, 10, 5440–5445.
- (23) Diemann, E.; Mueller, A.; Aymonino, P. J. The thermal decomposition of  $(NH_4)_2Mo_3S_{13}$ . $H_2O.nH_2O.$  Z. Anorg. Allg. Chem. **1981**, 479, 191–198.
- (24) Prasad, T. P.; Diemann, E.; Mueller, A. Thermal Decomposition of  $(NH_4)_2MoO_2S_2$ ,  $(NH_4)_2MoS_4$ ,  $(NH_4)_2WO_2S_2$  and  $(NH_4)_2WS_4$ . *J. Inorg. Nucl. Chem.* **1973**, 35, 1895–1904.
- (25) Kang, K.; Xie, S. E.; Huang, L. J.; Han, Y. M.; Huang, P. Y.; Mak, K. F.; Kim, C. J.; Muller, D.; Park, J. High-mobility three-atom-thick semiconducting films with wafer-scale homogeneity. *Nature* **2015**, *520*, 656–660.

- (26) Shomalian, K.; Bagheri-Mohagheghi, M. M.; Ardyanian, M. Synthesis and characterization of porous nanoparticles of molybdenum sulfide (MoS<sub>2</sub>) chalcogenide semiconductor prepared by polymerizing-complexing sol—gel method. *J. Mater. Sci.: Mater. Electron.* **2017**, 28, 14331.
- (27) Li, N.; Chai, Y.; Dong, B.; Liu, B.; Guo, H.; liu, C. Preparation of porous  $MoS_2$  viasol-gel route using  $(NH_4)_2Mo_3S_{13}$  as Precourosr. *Mater. Lett.* **2012**, *88*, 112–115.
- (28) Coleman, J. N.; Lotya, M.; O'Neill, A.; Bergin, S. D.; King, P. J.; Khan, U.; Young, K.; Gaucher, A.; De, S.; Smith, R. J.; Shvets, I. V.; Arora, S. K.; Stanton, G.; Kim, H. Y.; Lee, K.; Kim, G. T.; Duesberg, G. S.; Hallam, T.; Boland, J. J.; Wang, J. J.; Donegan, J. F.; Grunlan, J. C.; Moriarty, G.; Shmeliov, A.; Nicholls, R. J.; Perkins, J. M.; Grieveson, E. M.; Theuwissen, K.; McComb, D. W.; Nellist, P. D.; Nicolosi, V. Two-Dimensional Nanosheets Produced by Liquid Exfoliation of Layered Materials. *Science* 2011, 331, 568–571.
- (29) Zeng, Z. Y.; Yin, Z. Y.; Huang, X.; Li, H.; He, Q. Y.; Lu, G.; Boey, F.; Zhang, H. Single-Layer Semiconducting Nanosheets: High-Yield Preparation and Device Fabrication. *Angew. Chem., Int. Ed.* **2011**, *50*, 11093–11097.
- (30) Wang, X.; Feng, H.; Wu, Y.; Jiao, L. Controlled synthesis of highly crystalline MoS<sub>2</sub> flakes by chemical vapor deposition. *J. Am. Chem. Soc.* **2013**, *135*, 5304–5307.
- (31) Uzcanga, I.; Bezverkhyy, I.; Afanasiev, P.; Scott, C.; Vrinat, M. Sonochemical preparation of  $MoS_2$  in aqueous solution: Replication of the cavitation bubbles in an inorganic material morphology. *Chem. Mater.* **2005**, *17*, 3575–3577.
- (32) Tian, Y.; He, Y.; Zhu, Y. F.; Wang, W. Hydrothermal synthesis of  $MoS_2$  and its lubricating properties. *Acta Phys-Chim. Sin.* **2003**, *19*, 1044-1048.
- (33) Tian, Y. M.; Liu, Y. H.; Sheng, Y.; Zhao, J. Z.; Jiang, Y. Q.; Wang, Z. C. Facile route to synthesis of MoS<sub>2</sub> nanorods additive. *Abstr. Pap. Am. Chem. Soc.* **2005**, 229, U913—U913.
- (34) Guo, B.; Yu, K.; Li, H.; Song, H.; Zhang, Y.; Lei, X.; Fu, H.; Tan, Y.; Zhu, Z. Hollow Structured Micro/Nano MoS<sub>2</sub> Spheres for High Electrocatalytic Activity Hydrogen Evolution Reaction. *ACS Appl. Mater. Interfaces* **2016**, *8*, 5517–5525.
- (35) Massey, A. T.; Gusain, R.; Kumari, S.; Khatri, O. P. Hierarchical Microspheres of MoS<sub>2</sub> Nanosheets: Efficient and Regenerative Adsorbent for Removal of Water-Soluble Dyes. *Ind. Eng. Chem. Res.* **2016**, *55*, 7124–7131.
- (36) Zelenski, C. M.; Dorhout, P. K. Template synthesis of nearmonodisperse microscale nanofibers and nanotubules of MoS<sub>2</sub>. *J. Am. Chem. Soc.* **1998**, 120, 734–742.
- (37) Muller, A.; Sarkar, S.; Bhattacharyya, R. G.; Pohl, S.; Dartmann, M. Directed Synthesis of  $[Mo_3S_{13}]^{2}$ , an Isolated Cluster Containing Sulfur-Atoms in 3 Different States of Bonding. *Angew. Chem., Int. Ed. Engl.* **1978**, *17*, 535–535.
- (38) Moulder, J. F.; Stickle, W. F.; Sohol, P. E.; Bomben, K. D. *Handbook of X-ray Photoelectron Spectroscopy*; Physical Electronics, Inc.: Eden Prairie, MN, 1995.
- (39) Kibsgaard, J.; Jaramillo, T. F. Molybdenum Phosphosulfide: An Active, Acid-Stable, Earth-Abundant Catalyst for the Hydrogen Evolution Reaction. *Angew. Chem., Int. Ed.* **2014**, *53*, 14433–14437.
- (40) Li, H.; Zhang, Q.; Yap, C. C. R.; Tay, B. K.; Edwin, T. H. T.; Olivier, A.; Baillargeat, D. From Bulk to Monolayer  $MoS_2$ : Evolution of Raman Scattering. *Adv. Funct. Mater.* **2012**, 22, 1385–1390.
- (41) Li, N.; Chai, Y.; Dong, B.; Liu, B.; Guo, H.; Liu, C. Preparation of porous  $MoS_2$  via a sol–gel route using  $(NH_4)_2Mo_3S_{13}$  as precursor. *Mater. Lett.* **2012**, *88*, 112–115.
- (42) Skrabalak, S. E.; Suslick, K. S. Porous MoS2 Synthesized by Ultrasonic Spray Pyrolysis. J. Am. Chem. Soc. 2005, 127, 9990—9991.
- (43) Evans, B. L.; Young, P. A. Optical Absorption and Dispersion In Molybdenum Disulphide. *Proc. R. Soc. London, Ser. A* **1965**, 284, 402–422.
- (44) Wilcoxon, J. P.; Newcomer, P. P.; Samara, G. A. Synthesis and optical properties of MoS<sub>2</sub> and isomorphous nanoclusters in the quantum confinement regime. *J. Appl. Phys.* **1997**, *81*, 7934–7944.